Ataluren and aminoglycosides stimulate read-through of nonsense codons by orthogonal mechanisms

Martin Y. Ng[a], Hong Li[a], Mikel D. Ghelfi[a], Yale E. Goldman[b], and Barry S. Cooperman[a,1]

[a]Department of Chemistry, University of Pennsylvania, Philadelphia, PA 19104; and [b]Department of Physiology, Perelman School of Medicine, University of Pennsylvania, Philadelphia, PA 19104

Edited by Peter B. Moore, Yale University, New Haven, CT, and approved December 3, 2020 (received for review October 2, 2020)

During protein synthesis, nonsense mutations, resulting in premature stop codons (PSCs), produce truncated, inactive protein products. Such defective gene products give rise to many diseases, including cystic fibrosis, Duchenne muscular dystrophy (DMD), and some cancers. Small molecule nonsense suppressors, known as TRIDs (translational read-through–inducing drugs), stimulate stop codon read-through. The best characterized TRIDs are ataluren, which has been approved by the European Medicines Agency for the treatment of DMD, and G418, a structurally dissimilar aminoglycoside. Previously [1], we applied a highly purified in vitro eukaryotic translation system to demonstrate that both aminoglycosides like G418 and more hydrophobic molecules like ataluren stimulate read-through by direct interaction with the cell's protein synthesis machinery. Our results suggested that they might do so by different mechanisms. Here, we pursue this suggestion through a more-detailed investigation of ataluren and G418 effects on read-through. We find that ataluren stimulation of read-through derives exclusively from its ability to inhibit release factor activity. In contrast, G418 increases functional near-cognate tRNA mispairing with a PSC, resulting from binding to its tight site on the ribosome, with little if any effect on release factor activity. The low toxicity of ataluren suggests that development of new TRIDs exclusively directed toward inhibiting termination should be a priority in combatting PSC diseases. Our results also provide rate measurements of some of the elementary steps during the eukaryotic translation elongation cycle, allowing us to determine how these rates are modified when cognate tRNA is replaced by near-cognate tRNA ± TRIDs.

nonsense suppression | read-through | TRID | ataluren | G418

Premature stop codons (PSCs) arise in messenger RNA (mRNA) as a consequence of nonsense mutations. Such mutations lead to the replacement of an amino acid codon in mRNA by one of three stop codons—UAA, UGA, or UAG (2–4)—and typically result in inactive truncated protein products. Nonsense mutations constitute ∼20% of transmitted or de novo germline mutations (5–7). Globally, there are ∼7,000 known genetically transmitted disorders in humans, and ∼12% of all human disease mutations are nonsense mutations (8). Clearly, millions of people worldwide would benefit from effective therapies directed toward PSC suppression. PSC disorders can, in principle, be treated with therapeutic agents that induce the selection of near-cognate transfer RNAs (tRNAs) at the PSC position and insertion of the corresponding amino acids into the nascent polypeptide. This process, referred to as "read-through," restores the production of full-length functional proteins, albeit at levels considerably reduced from wild type. However, even low rates of read-through can improve clinical outcomes when essential proteins are completely absent.

The best characterized therapeutic agents inducing read-through, currently referred to as TRIDs [translational read-through–inducing drugs (9)], are ataluren (Translarna), a hydrophobic substituted oxadiazole, and the highly polar class of aminoglycoside antibiotics (AGs) (10). Only ataluren has been approved for clinical use. This approval has come from the European Medicines Agency, although not yet from the US Food and Drug Administration, and is currently specified for treatment of patients with nonsense-mediated Duchenne muscular dystrophy. However, clinical trials are underway for ataluren treatment of other diseases (aniridia, NCT02647359; epilepsy, NCT0275826; and colorectal and endometrium cancers, NCT04014530). The clinical utility of aminoglycosides has been restricted, in part, by their toxicities, which can arise from read-through of normal stop codons and other effects (3, 4, 11–14). Nevertheless, a Phase 2 clinical trial has recently begun (cystic fibrosis, NCT04135495) with a molecularly engineered AG, ELX-02 (formerly known as NB124), having much reduced toxicity (15).

Efforts to optimize AG design for clinical use as a TRID have benefited from the detailed understanding of how AGs promote misreading of near-cognate tRNAs, a process similar to read-through of stop codons. Such understanding has been gained from structural and mechanistic studies of the functional consequences of AG interaction with specific sites of bacterial ribosomes (16–22) and similar structural but sparser mechanistic studies on eukaryotic ribosomes (1, 23, 24). In contrast, much less is known about the mechanism by which ataluren stimulates read-through, and clear identification of the site(s) within the protein synthesis apparatus with which it interacts is completely lacking.

Significance

Nonsense mutations giving rise to premature stop codons (PSCs) cause many diseases, creating the need to develop safe and effective translational read-through–inducing drugs (TRIDs). The current best-characterized TRIDs are ataluren and aminoglycosides. Only ataluren has been approved for clinical use, albeit in a limited context. Here, we provide rate measurements of elementary steps in a single eukaryotic translation elongation cycle, allowing us to demonstrate that ataluren and the aminoglycoside G418 employ orthogonal mechanisms in stimulating PSC read-through: ataluren by inhibiting release factor-dependent termination of protein synthesis and G418 by increasing functional near-cognate transfer RNA mispairing, which permits continuation of synthesis. We conclude that development of new TRIDs combatting PSC diseases should prioritize those directed toward inhibiting termination.

Author contributions: M.Y.N., Y.E.G., and B.S.C. designed research; M.Y.N., H.L., and M.D.G. performed research; M.Y.N., Y.E.G., and B.S.C. analyzed data; and B.S.C. wrote the paper.

The authors declare no competing interest.

This article is a PNAS Direct Submission.

[1]To whom correspondence may be addressed. Email: cooprman@sas.upenn.edu.

This article contains supporting information online at https://www.pnas.org/lookup/suppl/doi:10.1073/pnas.2020599118/-/DCSupplemental.

Published January 7, 2021.

Recently (1), we reported results using a highly purified, eukaryotic cell–free protein synthesis system to examine the concentration effects of a dozen TRIDs on eukaryotic read-through activity. We denote our system PURE-LITE to differentiate it from the more complete PURE systems that have been developed for bacterial (25) and eukaryotic protein synthesis (26). PURE-LITE employs only the following purified components: eukaryotic 80S ribosomes programmed with variants of the cricket paralysis virus (CrPV) internal ribosome entry site (IRES) mRNA (Fig. 1 *A* and *C*), which can synthesize polypeptides in the complete absence of protein initiation factors (Fig. 1 *A* and *B*) (27, 28); aminoacylated tRNA isoacceptors; elongation factors eEF1A and eEF2; and release factors eRF1 and eRF3. In our previous study (1), we used 80S ribosomes purified from shrimp cysts, translation factors eEF1A, eEF2, eRF1, and eRF3 from *Saccharomyces cerevisiae*, and aminoacylated tRNAs prepared from *S. cerevisiae* and *Escherichia coli* and demonstrated that, despite the heterogeneity of this system, the relative potencies of a series of AGs toward read-through were fully consistent between the PURE-LITE assay and cell-based assays. This result was not unexpected, given that eukaryotic translation factors have very strongly conserved structures (29–31) and charged tRNAs from one species typically form functional complexes with both eEF1A and ribosomes from a different species (32, 33). All of the results presented below were obtained using the same components.

In the PURE-LITE system, the arrival of a PSC into the 40S subunit portion of the tRNA A-site of an actively translating ribosome can lead either to termination of protein synthesis via hydrolysis of the P-site bound peptidyl-tRNA catalyzed by the eRF1/eRF3 complex or to read-through via mispairing at the termination codon by a near-cognate tRNA (Fig. 1 *C* and *D*). TRIDs can increase the amount of read-through product by inhibiting termination and/or increasing functional near-cognate tRNA mispairing with a PSC. Our prior results with the PURE-LITE system measuring the stimulation of read-through by several AGs are consistent with there being a single tight site of AG binding to the ribosome with half maximal effective concentration (EC_{50}) values ranging from 0.4 to 4 μM and with varying yields of read-through product. This site likely corresponds to the tight site of AG binding within the decoding center of eukaryotic ribosomes (24), which is similar to that observed for bacterial ribosomes (16–18). In contrast, ataluren and ataluren-like compounds (34) show S-shaped read-through concentration-dependent activity curves, suggesting multisite binding to the protein synthesis machinery, with EC_{50} values between 0.10 and 0.35 mM and generally lower yields of read-through product compared with those obtained with AGs. Another important difference is in the rate of read-through product formation, which is much higher for one of the more potent AGs, G418, than for ataluren. These differences led us to suggest that AGs and ataluren-like compounds might stimulate read-through by different mechanisms (1).

Here, we pursue this suggestion through a more detailed investigation of ataluren and G418 effects on read-through. We find that ataluren stimulation of read-through derives exclusively from its ability to inhibit release factor activity. In contrast, G418 increases functional near-cognate tRNA mispairing resulting from tight binding to its primary site on the ribosome, and such binding has little if any effect on release factor activity. Our results also provide rate measurements of some of the elementary steps in a single eukaryotic translation elongation cycle, allowing us to determine how these rates are modified when cognate ternary complex (TC) (aminoacyl-tRNA.eEF1A.GTP) is replaced by near-cognate TC in the presence or absence of TRIDs.

Results

Throughout this section, we refer to several ribosome complexes formed during translation of Trp-IRES mRNA and Stop-IRES mRNA, as defined in Table 1.

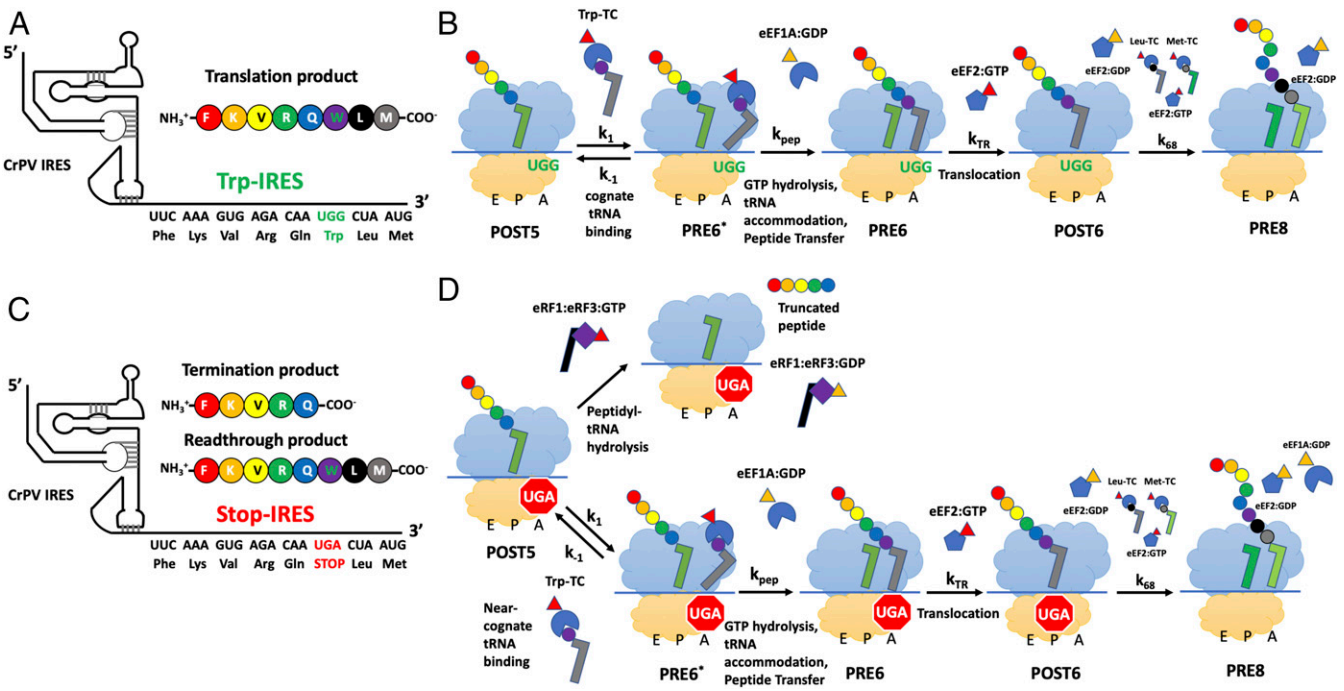

Fig. 1. CrPV-IRES mRNAs and elongation, read-through, and termination schemes. (*A*) Trp-IRES encodes PheLysValArgGlnTrpLeuMet. (*B*) Elongation reactions of Trp-POST5 complex. (*C*) Stop-IRES encodes PheLysValArgGlnStopLeuMet. (*D*) Termination and elongation (read-through) reactions of Stop-POST5 complex. Both Trp-POST5 and Stop-POST5 complexes contain PheLysValArgGln-$tRNA^{Gln}$ in the P-site. Rate constants are defined in the text.

Table 1. Ribosome complexes

Name	mRNA	A-site occupancy	P-site occupancy
Stop-POST5	Stop-IRES	—	FVKRQ-tRNA^{Gln}
Stop-PRE6		FVKRQW-tRNA^{Trp}	tRNA^{Gln}
Stop-POST6		—	FVKRQW-tRNA^{Trp}
Stop-PRE8		FVKRQWLM-tRNA^{Met}	tRNA^{Leu}
Trp-POST5	Trp-IRES	—	FVKRQ-tRNA^{Gln}
Trp-PRE6		FVKRQW-tRNA^{Trp}	tRNA^{Gln}
Trp-POST6		—	FVKRQW-tRNA^{Trp}
Trp-PRE8		FVKRQWLM-tRNA^{Met}	tRNA^{Leu}

Ataluren Only Stimulates Read-through in the Presence of eRF1/eRF3 and at Nonsaturating Concentrations of Trp-TC. Earlier we showed that read-through of the Stop-IRES mRNA UGA codon in the presence of release factors eRF1 and eRF3, as measured by the formation of the octapeptide FKVRQWLM from Stop-POST5, was stimulated by both ataluren and G418 (1). Importantly, the dependence of such stimulation on the concentration of eRF1/eRF3 (Fig. 2*A*) shows that, in the absence of eRF1/eRF3, ataluren does not stimulate basal read-through, while stimulation by G418 is pronounced. Raising eRF1/eRF3 concentration leads to complete loss of basal read-through (black line) and partial loss of G418-stimulated read-through (blue line). Added ataluren largely maintains both the original basal read-through level (green line) and the G418-stimulated level (pink line) over the concentration range of eRF1/eRF3 examined. Similarly, at a fixed eRF1/eRF3 concentration, ataluren stimulation of read-through diminishes as Trp-TC concentration is raised, while G418 stimulation is largely maintained (Fig. 2*B*). At fixed G418 concentration, the increase in octapeptide formation displays a sigmoidal dependence on added ataluren concentration (Fig. 2*C*), a point we return to below.

Ataluren Inhibits eRF1/eRF3 Peptidyl-tRNA Hydrolysis Activity; G418 Doesn't. The results presented in Fig. 2 *A* and *B* strongly suggest that ataluren inhibits eRF1/eRF3-dependent peptidyl-tRNA hydrolysis activity within Stop-POST5. This suggestion is confirmed by the results presented in Fig. 2*D* showing the dependence on ataluren concentration of such activity, as measured by the formation of FKVR[^{3}H]Q pentapeptide, which, unlike FKVR[^{3}H]Q-tRNA^{Gln}, dissociates from the ribosome on ultracentrifugation

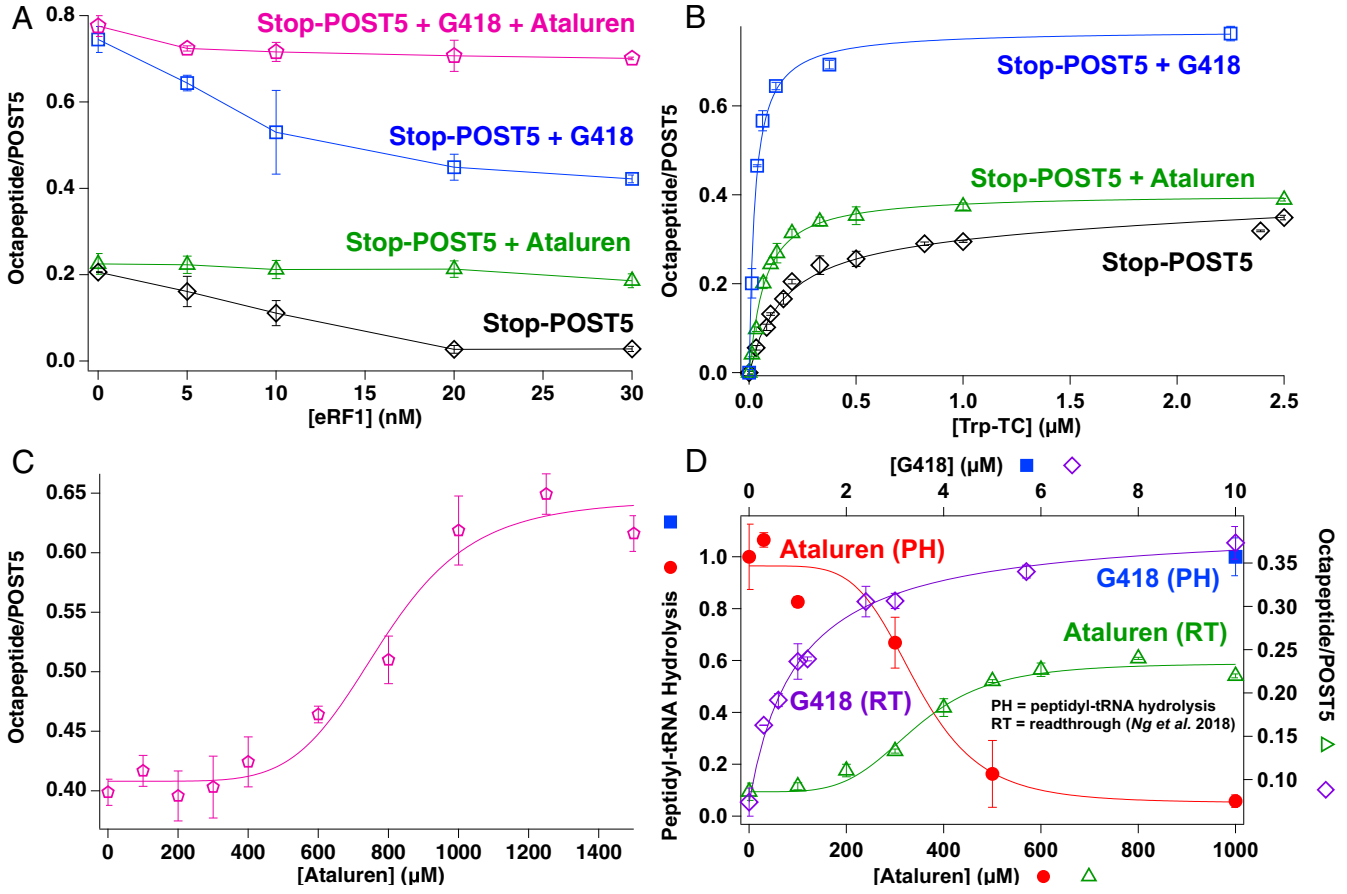

Fig. 2. Read-through and termination on mixing Stop-POST5 complex with other reactants. In these experiments, eRF3 concentration was always twice that of eRF1. (*A–C*) Octapeptide formation during stop codon read-through ± TRIDs, determined by [^{35}S]-FKVRQWLM-tRNA^{Met} cosedimenting with the ribosome as a function of (*A*) varying eRF1 concentration at fixed Trp-TC concentration, (*B*) varying Trp-TC concentration at fixed eRF1 concentration, and (*C*) varying ataluren concentration at fixed G418 concentration. Each of these experiments contained the following fixed concentrations: Stop-POST5 complex (0.02 μM), Leu-TC and [^{35}S]Met-TC (each 0.05 μM), GTP (1 mM), and, when present, G418 (10 μM). In addition, (*A*) contained 0.05 μM Trp-TC and varying eRF1; (*B*) contained 10 nM eRF1 and varying Trp-TC; and (*C*) contained 0.05 μM Trp-TC, 30 nM eRF1, and varying ataluren. (*D*) Direct comparison of ataluren (green Δ) and G418 (purple ♢) effects on octapeptide read-through, as demonstrated previously (1), and termination (eRF1/RF3-catalyzed pentapeptidyl-tRNA hydrolysis) (ataluren, red •; G418, blue ■). Stop-POST5 (0.05 μM) was mixed with Trp-TC, Leu-TC, and [^{35}S]Met-TC (each 0.05 μM), GTP (1 mM), 0.1 μM eRF1, 0.2 μM eRF3, and either ataluren (500 μM) or G418 (10 μM). The concentration of G418 is plotted on the top axis and of ataluren on the bottom axis. The fraction of peptidyl-tRNA hydrolyzed is plotted on the left axis, and the read-through product expressed as octapeptide/POST5 is plotted on the right axis.

(see *Materials and Methods*). The nonhyperbolic nature of the inhibition curve (solid red circles), suggestive of more than one site of ataluren interaction with the components of the release assay, parallels the S-shaped dependence of ataluren-stimulated read-through (open green triangles) (Fig. 2*C*). In contrast, G418, added at a concentration (10 μM) that is saturating for its stimulation of read-through (open purple diamonds), had little or no effect on release activity (solid blue square). Other ataluren-like TRIDs show similar S-shaped inhibition of eRF1/eRF3 release activity (*SI Appendix*, Fig. S1).

Kinetic Studies of POST5 to POST6 Conversion. Our earlier results (1) demonstrated that formation of the octapeptidyl-tRNA (FKVRQWLM-tRNA^{Met}) from Stop-POST5 proceeded much more slowly in the presence of ataluren than in the presence of G418 and that the rate-determining step in the ataluren-stimulated process corresponded to the conversion of Stop-POST5 to Stop-POST6. These results raise the question of which step (or steps) within this elongation cycle is (are) responsible for the slowness of ataluren-stimulated read-through of the UGA codon. To address this question, we measured rates of several different processes, as described below.

Trp-TC Interaction with POST5 Complexes. Rates of Trp-TC interaction with POST5 complexes were determined by the increase in proflavin (prf) fluorescence on rapid mixing of prf-labeled Trp-TC with either Stop-POST5 in the presence of G418 (Fig. 3*A*, blue line) or Stop-POST5 complex in the presence (green line) or absence (black line) of ataluren. These fluorescence increases parallel similar increases seen on binding of prf-labeled TCs to *E. coli* ribosomes (35). Repeating these measurements at varying POST5 concentrations (Fig. 3*B* and *SI Appendix*, Fig. S2 *A* and *B*) shows clear evidence for biphasic kinetics for Stop-POST5 complex interaction with Trp-TC. Traces were fit to Eq. **1**, where ΔF(t) and F_∞ denote the time-dependent fluorescence change and final fluorescence change at infinite time, respectively. To allow for comparisons, the results obtained with Trp-POST5 complex (*SI Appendix*, Fig. S2*C*) were also fit to Eq. **1**, although adequate fits were also obtained using a single exponential component:

$$\Delta F(t) = F_\infty - \left(F_1 e^{-k_{app,1}t} + F_2 e^{-k_{app,2}t}\right). \quad [1]$$

In all four cases, Trp-POST5 and Stop-POST5 in the presence of G418 or ± ataluren, values of $k_{app,1}$ were linearly dependent on POST5 concentration (Fig. 3*C*), suggesting that the slope of the line measures the second-order rate constant of Trp-TC binding to POST5 complex (k_1) and the Y-intercept measures the rate constant for Trp-TC dissociation (k_{-1}). In contrast, $k_{app,2}$ values show very little POST5 concentration dependence (Fig. 3*D*),

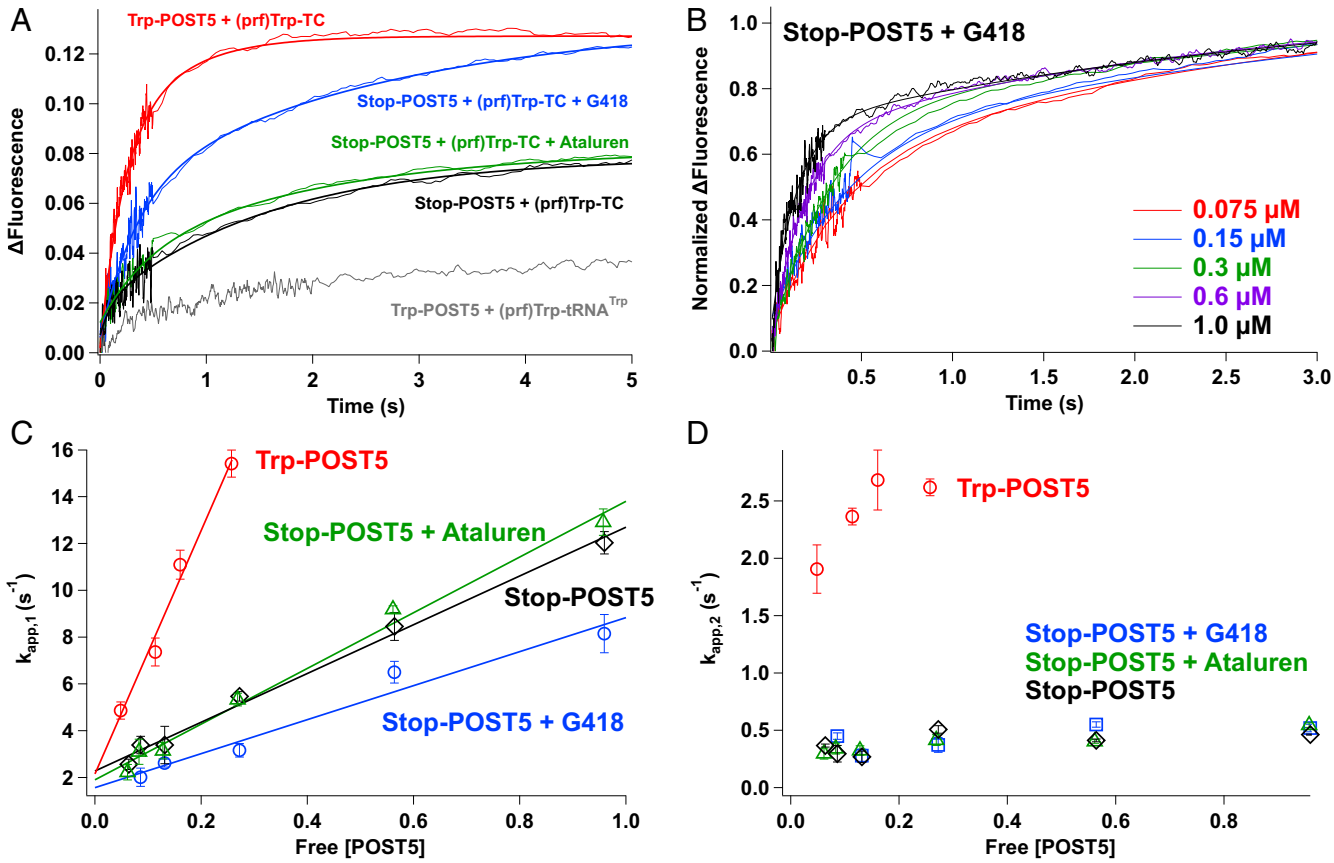

Fig. 3. Kinetics of (prf)Trp-TC binding to POST5 complexes. Experiments were carried out with fixed concentrations of (prf)Trp-TC (0.05 μM), 1 mM GTP, and, when added, 500 μM ataluren or 10 μM G418. (*A*) The increase in fluorescence intensity, measured as the voltage detected by the photomultiplier tube on the stopped-flow spectrofluorometer, following rapid mixing of (prf)Trp-TC with Trp-POST5 (0.075 μM, red line) or Stop-POST5 (0.075 μM) in the presence of either G418 (blue line) or ataluren (green line) or in the absence of TRID (black line). These increases are much larger than the small increase observed (gray line) on rapid mixing of 0.075 μM Trp-POST5 with 0.05 μM Trp-tRNA^{Trp}(prf) in the absence of eEF1A. (*B*) Normalized fluorescence changes of (prf)Trp-TC mixed with 0.075 to 0.30 μM added Stop-POST5 in the presence of G418. Changes for (prf)Trp-TC mixing with either Stop-POST5 ± ataluren or Trp-POST5 are shown in *SI Appendix*, Fig. S2. Dependence of (*C*) $k_{app,1}$ and (*D*) $k_{app,2}$ on free POST5 complex concentration, calculated as presented in *Materials and Methods*.

suggesting that they correspond to one or more first-order steps following Trp-TC binding, with an overall rate constant at saturating Trp-TC concentration of k_2. Values of k_1, k_{-1}, K_D (= k_{-1}/k_1), and k_2 are listed in Table 2. These values demonstrate that Trp-TC binds four to five times more weakly to Stop-IRES than to Trp-IRES, due to lower values of k_1, and that k_2 for Stop-IRES ± TRIDs is approximately fivefold slower than for Trp-IRES.

PRE6 Complex Formation as Measured by FKVRQW-tRNA^{Trp} Formation. Apparent rate constants of PRE6 formation on mixing varying Trp-TC concentrations with POST5 complex were determined using a rapid quench procedure. Sample results obtained at a single Trp-TC concentration (0.15 μM) are shown in Fig. 4*A*, permitting determination of $k_{app,pep}$ by fitting to a single exponential. The dependence of $k_{app,pep}$ values on Trp-TC concentration (Fig. 4*B*) permitted calculation of k_{pep} values (Table 2), demonstrating that PRE6 formation proceeds with the same rate constant from Trp-POST5 and Stop-POST5 in the presence of G418 but is four to five times slower from Stop-POST5 ± ataluren. Importantly, although added ataluren does not significantly increase k_{pep}, it does significantly increase the amount of Stop-PRE6 complex formed in the presence of eRF1/eRF3 at a non-saturating concentration of Trp-TC (Fig. 4*A*). This is consistent with ataluren's increase of Stop-PRE8 complex formed at non-saturating concentrations of Trp-TC in the presence of eRF1/eRF3 (Fig. 2 *A* and *C*).

PRE6 to POST6 Conversion (Translocation). We used three different approaches to estimate the rate constant for PRE6 complex conversion to POST6 complex. In these experiments, we used a saturating concentration (0.5 μM) either of Trp-TC, when POST5 complex was limiting, or of POST5 complex, when Trp-TC was limiting.

Approach one involved monitoring the eEF2-dependent increase in Trp-tRNA^{Trp}(prf) fluorescence on rapid mixing of Trp-TC and eEF2 with Trp-POST5, paralleling similar experiments used in measuring translocation on *E. coli* ribosomes (36–38). Here, the rapid initial biphasic rise that is seen in the absence of eEF2 (Fig. 3 *A* and *B*) is followed by a slower, eEF2-dependent rise corresponding to translocation of Trp-PRE6 to Trp-POST6 (Fig. 4*C*) and of Stop-PRE6 to Stop-POST6 in the presence of G418 (Fig. 4*D*). The traces obtained for these two cases were fit to Eq. **2**. As expected, only $k_{app,3}$ is eEF2 dependent, yielding values of K_m^{eEF2} (for Trp-POST6) and k_{TRfl} (defined as the value of k_{app3} at saturating eEF2) shown in Table 2:

$$\Delta F(t) = F_\infty - \left(F_1 e^{-k_{app,1}t} + F_2 e^{-k_{app,2}t} + F_3 e^{-k_{app,3}t}\right). \quad [2]$$

In contrast to the results obtained with Trp-PRE6 and Stop-PRE6 in the presence of G418, much less eEF2-dependent fluorescence increase was observed for Stop-PRE6 in the presence of ataluren or in the absence of any added TRID (Fig. 4*D*). However, translocation must have occurred, since Stop-POST6 is a required intermediate when Stop-POST5 is converted to Stop-PRE8 by the simultaneous addition of Trp-TC, Leu-TC, Met-TC, and eEF2 (Fig. 2*A*). The lack of an eEF2-dependent fluorescence change is due, at least in part, to the slow formation (see below) and lability of the Stop-POST6 complex ± ataluren (*SI Appendix*, Fig. S3).

For the second approach, we formally divided the conversion of a POST5 complex into a PRE8 complex, proceeding with an overall rate constant k_{58}, into three discrete steps (Scheme 1): 1) formation of PRE6 complex with rate constant k_{pep}, 2) translocation of PRE6 complex to POST6 complex with calculated rate constant k_{TRcalc}, and 3) conversion of POST6 complex to PRE8 complex with rate constant k_{68}, allowing evaluation of k_{TRcalc} from Eq. **3**. We determined k_{pep} as described above.

Table 2. Measured rate constants

	Trp	Stop	Stop	Stop
TRID	None	G418	Ataluren	None
k_1 ($\mu M^{-1} \cdot s^{-1}$)	52 ± 4	7± 1	12 ± 1	10 ± 1
k_{-1} (s^{-1})	2.2 ± 0.3	1.6 ± 0.4	1.9 ± 0.3	2.3 ± 0.2
$K_{D,TC}$ (μM)	0.042 ± 0.004	0.22 ± 0.04	0.16 ± 0.02	0.22 ± 0.02
k_2 (s^{-1})	2.7 ± 0.1	0.52 ± 0.03	0.55 ± 0.03	0.46 ± 0.02
k_{pep} (s^{-1})	0.30 ± 0.03	0.32 ± 0.03	0.07 ± 0.01	0.06 ± 0.01
$K_{m,pep}$ (μM)	0.30 ± 0.03	0.32 ± 0.03	0.2 ± 0.1	0.07 ± 0.02
k_{TRfl} (s^{-1})	0.31 ± 0.04*	0.30 ± 0.03*	n.d.†	n.d.†
k_{TRcalc} (s^{-1})	0.36 ± 0.04	0.39 ± 0.04	0.014 ± 0.002	0.017 ± 0.002
k_{TRpu} (s^{-1})	0.24 ± 0.10	n.d.†	n.d.†	n.d.†
K_m^{eEF2} (μM)	0.3 ± 0.1	n.d.†	n.d.†	n.d.†
k_{58} (s^{-1})	0.07 ± 0.01	0.057 ± 0.004	0.010 ± 0.001‡	0.011 ± 0.001‡
k_{68} (s^{-1})	0.12 ± 0.01	0.083 ± 0.003	0.12 ± 0.02‡	0.13 ± 0.01‡

Except for k_1 and k_{-1}, rate constant values reported are determined at saturating concentrations of either TCs or ribosome complexes, as appropriate. Rate constants for processes requiring eEF2 were performed either at a single eEF2 concentration (1 μM) or at 1 μM and a higher concentration as indicated. In all cases using two eEF2 concentrations, essentially identical results were obtained for both. Error ranges are average deviations of duplicate experiments.
*[eEF2] = 1 and 3 μM.
†Not determined.
‡[eEF2] = 1 and 4 μM.

$$k_{TRcalc}^{-1} = k_{58}^{-1} - \left(k_{pep}^{-1} + k_{68}^{-1}\right). \quad [3]$$

To determine k_{58}, we monitored octapeptide formation following mixing of POST5 complex with Trp-TC, Leu-TC, Met-TC, and eEF2. To determine k_{68}, we first preincubated POST5 complex with Trp-TC and eEF2 to form POST6, and then monitored octapeptide formation following rapid mixing with Leu-TC and Met-TC while maintaining eEF2 concentration. The results found for k_{58} and k_{68} are presented in Fig. 5 with rate constants listed in Table 2. Importantly, the values of k_{TRcalc} for both Trp-PRE6 and Stop-PRE6 in the presence of G418 agree quite well with the directly measured values of k_{TRfl}, supporting the use of Eq. **3** in determining the translocation rate constants for Stop-PRE6 ± ataluren. These rate constants, which are essentially identical to one another, are each 20 to 30 times slower than the rate constants determined for Trp-PRE6 and Stop-PRE6 in the presence of G418. Unsurprisingly, k_{68} is about the same for all four experiments (Table 2) since POST6 to PRE8 conversion proceeds with cognate aminoacyl-tRNAs in all cases.

Yields of PRE8 complex depended on the rate of PRE6 to POST6 translocation and the lability of the POST6 Complex. Trp-POST6 is formed relatively rapidly and is quite stable, so the high yield of Trp-PRE8 is unaffected by the duration of the preincubation step. In contrast, the lability of the Stop-POST6

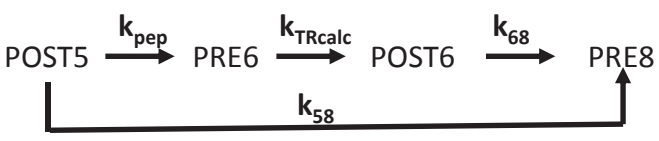

$$k_{TRcalc}^{-1} = k_{58}^{-1} - (k_{pep}^{-1} + k_{68}^{-1})$$

Scheme 1.

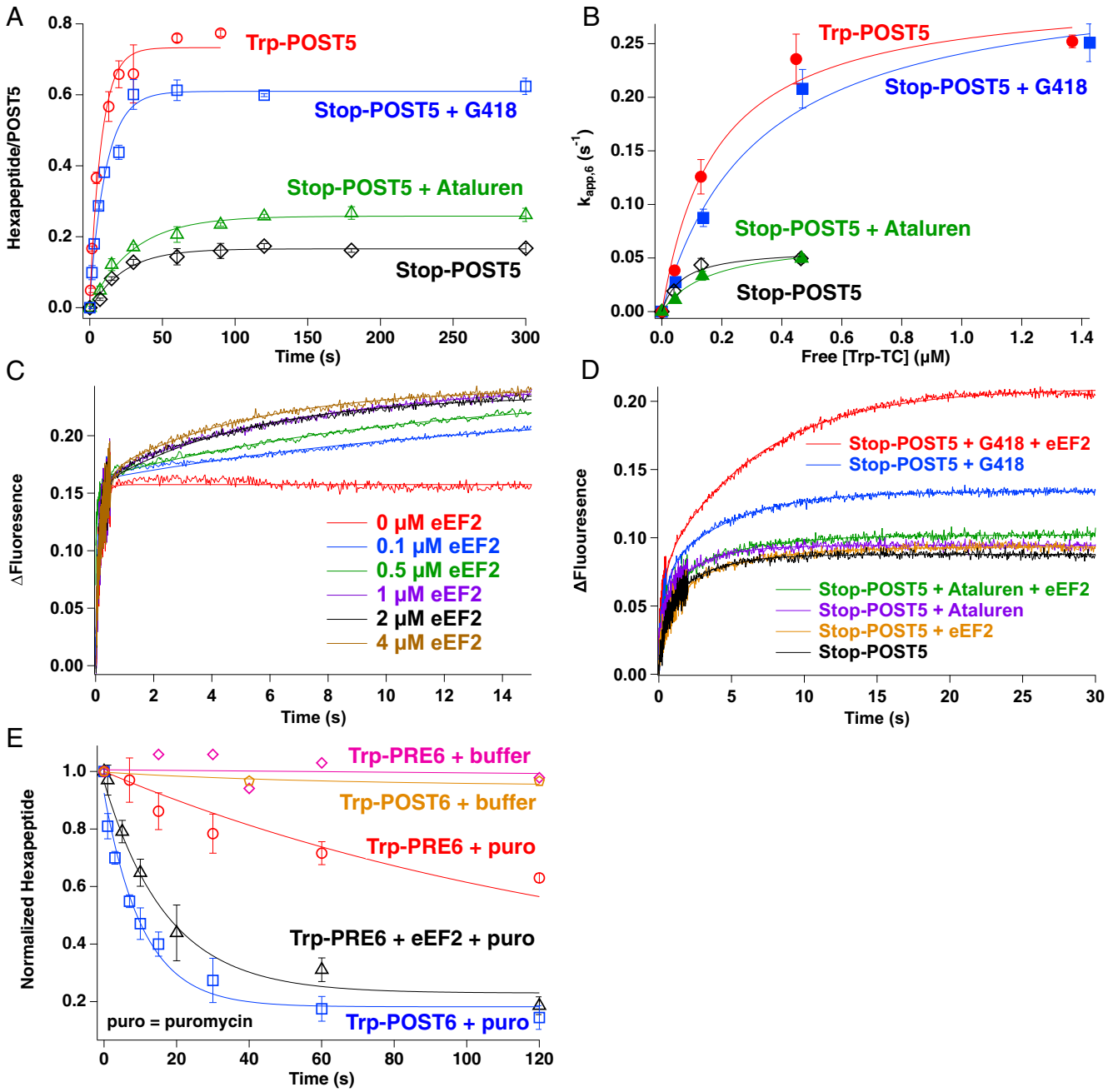

Fig. 4. Kinetics of PRE6 formation and translocation. (*A*) Rates of FKVRQW-tRNA^{Trp} formation were measured by TLE analysis following strong base quenching. POST5 complexes (0.02 μM) were rapidly mixed with [^{3}H]Trp-tRNA^{Trp} (0.15 μM), eEF1A (0.3 μM), eRF1 (0.02 μM), eRF3 (0.04 μM), and GTP (1 mM) in the presence of either G418 (10 μM) or ataluren (500 μM) or in the absence of TRIDs. Aliquots were quenched at various times with 0.4 M NaOH. (*B*) The dependence of apparent rate constants of FKVRQW-tRNA^{Trp} formation on free Trp-TC concentration, calculated as presented in *Materials and Methods*. (*C* and *D*) Rates of PRE6 translocation to POST6 were determined from the eEF2-dependent increase in prf fluorescence on rapid mixing of POST5 (0.15 μM) with (Prf)Trp-tRNA^{Trp} (0.05 μM), eEF1A (0.2 μM), GTP (1 mM), and eEF2. (*C*) Trp-PRE6 with varying eEF2 concentrations. (*D*) Stop-PRE6 ± TRID. Time-dependent changes in prf fluorescence on rapid mixing of Stop-POST5 (0.15 μM) with 1 μM eEF2 and either 10 μM G418 or 500 μM ataluren or in the absence of TRID. Raising the eEF2 concentration to 3 μM had negligible effects on the traces shown. For Stop-POST5 ± ataluren, extending the observations to 600 s gave no evidence of a significant eEF2-dependent change. (*E*) Rate of Trp-PRE6 translocation to Trp-POST6 as determined by FKVRQW-puromycin formation. Trp-PRE6 or Trp-POST6 (0.025 μM) was incubated with ±1 μM eEF2 and ±5 μM puromycin for various times and quenched with ice-cold pH 6 buffer. Hexapeptidyl-tRNA remaining on the ribosome was determined by cosedimentation.

complex ± TRIDs (*SI Appendix*, Fig. S3), presumably due to dissociation of FVKRQW-tRNA^{Trp} from the P-site, results in preincubation-induced reduction in the yields of Stop-PRE8. The higher overall yields of Stop-PRE8 found with G418 compared to those found ± ataluren are attributable to the much more rapid formation of Stop-POST6 in the presence of G418.

The third approach exploits the more rapid reaction with puromycin of POST6 versus PRE6 complexes, as described previously (39). As a consequence of this difference, the observed rate constant of puromycin–WQRVKF formation following the simultaneous addition of saturating eEF2 concentration (1 μM) and 5 μM puromycin to PRE6 (k_{obs}, 0.058 ± 0.003 s^{-1}) falls in

between the rate constants measured separately for puromycin reaction with Trp-PRE6 (k_{PRE}, 0.0070 ± 0.0004 s^{-1}) and Trp-POST6 (k_{POST}, 0.094 ± 0.004 s^{-1}) (Fig. 4*E*), allowing estimation of k_{TRpu} by fitting our results to Scheme 2.

Because of the labilities of Stop-POST6 ± TRIDs, this approach could only be applied to estimate the translocation rate constant of Trp-PRE6 (k_{TRpu}), yielding a value (Table 2) consistent with the values of k_{TRfl} and k_{TRcalc} but with a larger uncertainty due to accumulation of errors in the values of k_{obs}, k_{PRE}, and k_{POST}.

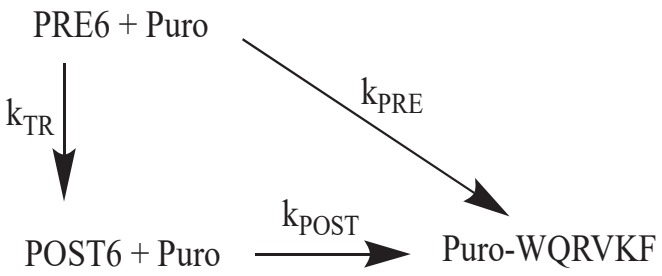

Scheme 2.

Discussion

Here, we demonstrate that ataluren stimulation of termination codon read-through derives exclusively from its ability to block termination (Fig. 1), diverting an increased amount of Stop-POST5, which contains a UGA stop codon in the A-site, toward elongation. This exclusivity is shown by ataluren's failure to stimulate basal read-through in the absence of eRF1/eRF3 (Fig. 2*A*) and its lack of effect on the measured rate constants for near-cognate TC binding, peptide bond formation, and translocation (Table 2). In contrast, G418 stimulates functional binding of near-cognate tRNAs at a stop codon by increasing the rate constants of peptide bond formation and translocation to levels similar to those found following TC binding to its cognate codon while not affecting termination at a concentration (10 μM) that is fully saturating with respect to its stimulation of read-through [EC_{50}, 0.98 μM (1)].

In addition to demonstrating the orthogonal mechanisms by which ataluren and G418 stimulate read-through, our results (Table 2) provide important information about the rates of some of the elementary steps in a single eukaryotic translation elongation cycle and how these rates are modified when the cognate UGG codon for $tRNA^{Trp}$ is replaced by the near-cognate UGA stop codon in the absence or presence of TRIDs. Also noteworthy is the lability of the near-cognate Stop-POST6 complex ± TRIDs, which contrasts markedly with the stability of the

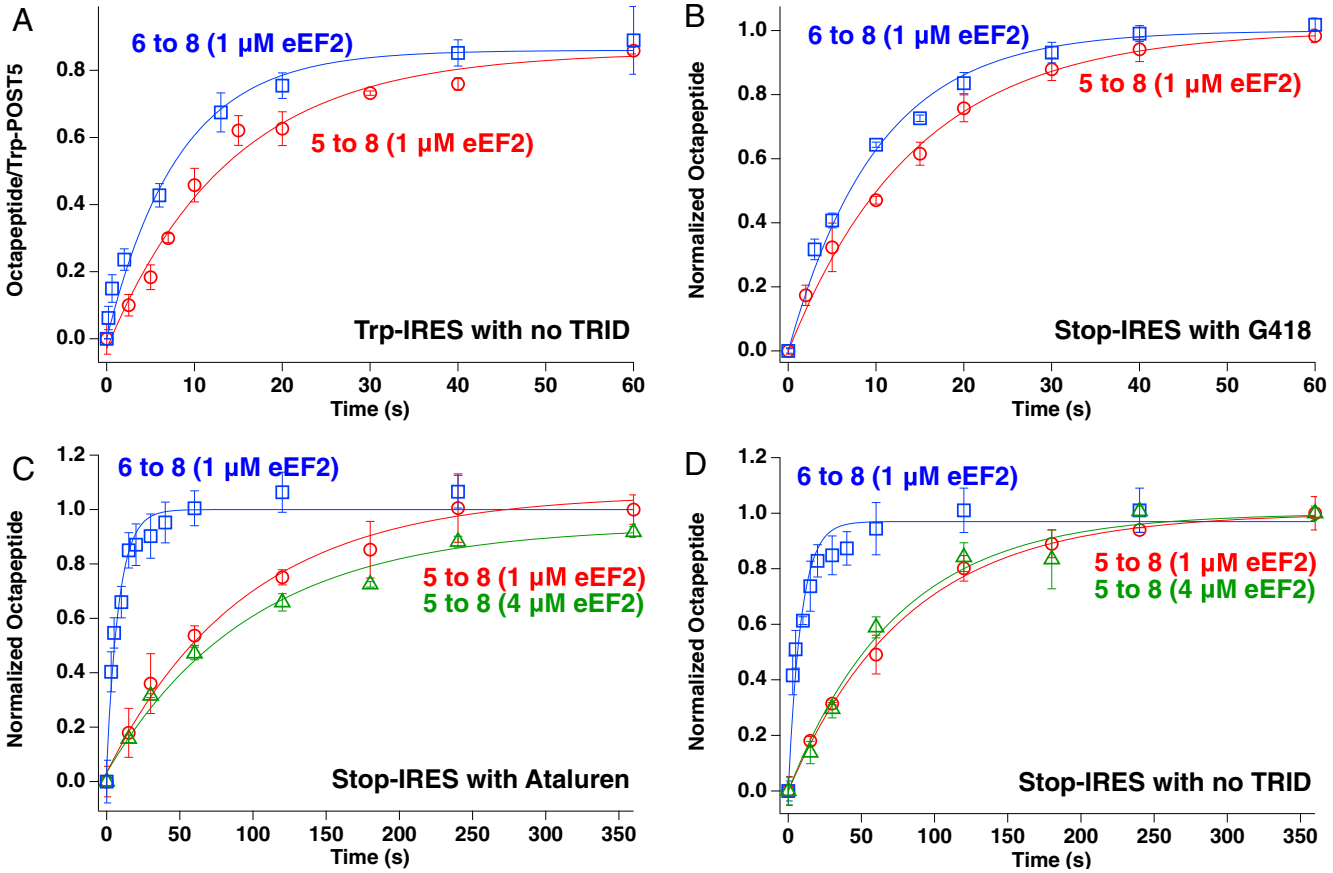

Fig. 5. Kinetics of octapeptide formation. Octapeptide formation was determined as described in Fig. 2. k_{58} and k_{68} were measured for (*A*) Trp-POST5, (*B*) Stop-POST5 + 10 μM G418, (*C*) Stop-POST5 + 600 μM ataluren, and (*D*) Stop-POST5, no added TRID. Measurements used to determine k_{58} are indicated as 5 to 8 in the figures and were carried out following mixing 0.02 μM POST5 complex with 0.5 μM each of Trp-TC, Leu-TC, and [^{35}S]-Met-TC, 1 μM or 4 μM eEF2 as indicated, and 1 mM GTP. Measurements used to determine k_{68} are indicated as 6 to 8 in the figures and were carried out similarly, except that 0.02 μM POST5 complex was premixed with 0.5 μM Trp-TC and 1 μM eEF2 concentration for either 20 s (*A* and *B*) or 2 min (*C* and *D*), followed by further mixing with 0.5 μM each of Leu-TC and [^{35}S]Met-TC while maintaining eEF2 concentration. Octapeptide yields were normalized to 0.79 (k_{58}) and 0.61 (k_{68}) for *B*, 0.42 (k_{58}) and 0.33 (k_{68}) for *C*, and 0.42 (k_{58}) and 0.34 (k_{68}) for *D*. Increasing eEF2 concentration from 1 to 4 μM had negligible effects on octapeptide yield.

cognate Trp-POST6 complex (*SI Appendix*, Fig. S3). For the cognate case, Trp-POST5 conversion to Trp-POST6, k_{pep}, and k_{TR} are similar, so both overall peptide formation and translocation are partially rate determining. Both of these rate constants are strongly decreased in the near-cognate case, Stop-POST5 conversion to Stop-POST6. The decrease is much larger for k_{TR} (20- to 30-fold) than for k_{pep} (5-fold), such that translocation becomes almost fully rate determining. This large effect on k_{TR} parallels the similar large translocation rate differences on switching from cognate to near-cognate tRNA, 10- to 80-fold, recently observed in bacterial elongation (40). On the other hand, the fivefold decrease in k_{pep} found here is more modest than the negative effects reported for bacterial ribosomes [40- to 80-fold, Gromadski and Rodnina (20)]. The less-dramatic effect of the near-cognate codon that we observe on k_{pep} may be due to the sequence context we employ for the stop codon, which optimizes the efficiency of read-through (1), facilitating the quantification of TRID effects. Adding G418 increases k_{pep} (fivefold) and k_{TR} (20-fold) for near-cognate elongation up to levels similar to those seen for cognate elongation. Adding the AG streptomycin increases bacterial near-cognate k_{pep} to a similar extent [10-fold (20)]. However, our results measuring the effects of G418 on eukaryotic translocation run counter to a study (40) showing that adding the AG paromomycin (10 μM) markedly inhibits bacterial translocation of both a cognate peptidyl-tRNA (16-fold), and a wobble base near-cognate tRNA (threefold). In contrast, our results show that G418 (10 μM) strongly stimulates translocation of a wobble base near-cognate peptidyl-tRNA (20-fold, Table 2) and provide clear evidence that G418 has no major effect on cognate peptidyl-tRNA translocation, a point discussed more fully in *SI Appendix*. Determining whether these apparent discrepancies reflect differences in the mechanisms of action of paromomycin, a tetrasaccharide, and G418, a trisaccharide, in the structural dynamics of the protein synthesis machinery of eukaryotic versus bacterial ribosomes and/or in the tRNAs employed would require further study. Additional relevant results previously reported for bacterial elongation are provided in *SI Appendix*, Table S1.

Our overall rate constant for an elongation cycle at saturating TC in the cognate case [~0.15 to 0.25 s^{-1}, this work and Zhang et al. (39)] is similar to the average value of ~0.06 to 0.1 s^{-1}, measured at 26 °C, which can be calculated from results presented in studies in which all components of the protein synthesis machinery are prepared from *S. cerevisiae* (41, 42). These values are much lower than those for minimal in vitro bacterial systems [~3 s^{-1} at saturating TC, 25 °C (38, 43)] or for in vivo eukaryotic elongation [3 to 5 s^{-1} (44)], likely reflecting, at least in part, the absence of eukaryotic factors essential for efficient catalysis in these minimal systems (39). Thus, for example, Bugaud et al. (45) report a rate constant of ~0.7 s^{-1} at ~30 °C in a rabbit reticulocyte extract, which may contain such factors. It is not unlikely that bacterial elongation is less dependent on such additional factors. Additionally, in vitro elongation rates in minimal systems can vary significantly as a function of buffer composition, which we have not optimized in this work.

Are the in vitro results presented here indicative of ataluren's effect in cells and relevant for ongoing efforts to develop new, more potent TRIDs as therapies for PSC diseases (10, 13, 46–49)? Supporting cell biological and health care relevance is the straightforward manner in which restricting ataluren's effect to inhibition of termination explains its lack of stimulation of misreading at normal codons in cellular assays (50). A possible concern is that the ataluren EC_{50} value in our assays (~300 μM, Fig. 2*D*) is ~10 to 30 times higher than ataluren concentrations employed in the growth media typically used in studies of ataluren stimulation of read-through in intact cells or tissue cultures (50, 51). This difference may be more apparent than real, since it is quite plausible that ataluren, like other hydrophobic molecules, is preferentially taken up by cells, such that its cellular concentration far exceeds that present in the cell culture medium (52). At present, we are unaware of any published work on this point, but it clearly will be of interest to determine how ataluren uptake varies by cell type.

Despite this uncertainty, the low toxicity of ataluren in clinical studies coupled with our results suggests that development of new TRIDs exclusively directed toward inhibiting termination should receive priority for combatting PSC diseases. In addition, the orthogonality of ataluren and G418 effects on read-through creates the opportunity for additivity between these two TRIDs. This potential is realized in the results presented in Fig. 2*C*, demonstrating the ability of ataluren to enhance G418-stimulated read-through via its inhibition of termination. Combining AGs with ataluren or ataluren-like molecules might result in lowering the doses of both agents required for effective treatment of PSC diseases, thereby reducing side effects. Other small hydrophobic compounds have been found to potentiate AG-stimulated read-through in breast cancer cells (53), although such stimulation probably does not involve inhibition of termination.

Materials and Methods

Materials.

Ribosomes and IRES mRNAs. The 40S and 60S ribosome subunits from shrimp (*Artemia salina*) cysts, Trp-IRES and Stop-IRES, were prepared as described (1, 39). 70S ribosomes from MRE600 *E. coli* were prepared by subjecting the S100 fraction to ultracentrifugation at 30,000 rpm (104,000 Å~ *g*) in a Type 45 Ti rotor for 21 h at 4 °C in a buffer [20 mM Tris-HCl pH 7.5, 100 mM NH_4Cl, 10 mM $Mg(Ac)_2$, 0.5 mM ethylene diamine tetraacetic acid (EDTA) and 3 mM β-mercaptoethanol] layered on top of a 1.1 M sucrose cushion. The resulting 70S pellet was dissolved in 70S storage buffer [50 mM Tris·HCl pH 7.5, 70 mM NH_4Cl, 30 mM KCl, 7 mM $Mg(Ac)_2$, 0.5 mM EDTA, and 1 mM dithiothreitol (DTT)] and subjected to ultracentrifugation as above. The latter step was repeated an additional time and the final pellet was redissolved in 70S storage buffer and stored in small aliquots at −80 °C until use.

Yeast eEF1A and eEF2. Yeast eEF1A and eEF2 preparations were adapted from the eEF2 preparation method described previously (1, 54). Briefly, clarified lysate (150 mL) from fresh yeast cake in Buffer 1 (20 mM Hepes-KOH, pH 7.2, 10% glycerol, 5 mM $MgCl_2$, and 1 mM DTT), supplemented with 300 mM KCl, 1 mM PMSF, and 10 protease inhibitor mini tablets, was dialyzed against Buffer 1 overnight at 4 °C. Following filtration, the resulting solution (~150 mL) was loaded onto a 10-mL SOURCE 15S-column (GE Life Sciences) pre-equilibrated with Buffer 1 supplemented with 20 mM KCl. Using a linear gradient of 20 mM to 150 mM KCl in Buffer 1 resulted in separation of eEF2 and eEF1A, which eluted at 20 mM KCl and 90 mM KCl, respectively. eEF1A was used without further purification. The pooled eEF2 fraction was loaded onto an 8-mL SOURCE 15Q-column (GE Life Sciences) from which eEF2 was eluted using a linear gradient of 40 mM to 500 mM KCl in 20 mM Tris·HCl, pH 7.6, 10% glycerol, 5 mM $MgCl_2$, and 1 mM DTT.

Yeast eRF1/eRF3. Full-length eRF1 and eRF3 open reading frame sequences were inserted into the pET-15b (Novagen) plasmid obtained from the laboratory of Allan Jacobson (University of Massachusetts Medical School). eRF1 and eRF3 plasmids were transformed into BL21(DE3) CodonPlus (Agilent) strain in the presence of ampicillin. eRF1 and eRF3 were isolated from cell lysate using a protocol described earlier (55).

TRIDs. Atalauren sodium salt, GJ072, RTC13, and APOBA (3-[5-(4-azidophenyl)-1,2,4-oxadiazol-3-yl]-benzoic acid) were obtained as gifts from PTC Therapeutics. G418 was obtained from Sigma-Aldrich.

tRNAs. Yeast $tRNA^{Phe}$ was purchased from Sigma-Aldrich. Other isoacceptor tRNAs were prepared from bulk tRNA (Roche) from either *E. coli* ($tRNA^{Val}$, $tRNA^{Lys}$, $tRNA^{Gln}$, and elongator $tRNA^{Met}$) or yeast ($tRNA^{Arg}$, $tRNA^{Trp}$, and $tRNA^{Leu}$) via hybridization to immobilized complementary oligoDNAs as described previously (1, 39). *E. coli* and yeast tRNAs were charged with their cognate amino acids as described (56, 57). *E. coli* $tRNA^{Gln}$ was charged with either [^{3}H]-Gln for the peptide release assay or [^{14}C]-Gln for the Trp-$tRNA^{Trp}$(Prf) binding assay. Yeast $tRNA^{Trp}$ was charged with [^{3}H]-Trp for the hexapeptide assay or the hexapeptidyl-tRNA dissociation assay. *E. coli* elongator $tRNA^{Met}$ was charged with [^{35}S]-Met for the octapeptide formation assay.

POST5 complexes. This procedure is adapted from Ng et al. (1). All steps were performed in Buffer 4 (40 mM Tris HCl, pH 7.5, 80 mM NH_4Cl, 5 mM $Mg(Ac)_2$, 100 mM KOAc, and 3 mM β-mercaptoethanol). 80S-IRES complex was formed by incubating 0.8 μM 40S, 1.1 μM 60S, and 0.8 μM IRES at 37 °C for 2 min.

POST5 complex was formed by incubating 0.4 μM 80S-IRES with 0.4 μM each of Phe-tRNA^{Phe}, Lys-tRNA^{Lys}, Val-tRNA^{Val}, Arg-tRNA^{Arg}, and Gln-tRNA^{Gln}, 0.4 μM eEF1A, 1.0 μM eEF2, and 1 mM GTP at 37 °C for 25 min. POST5 was then purified by layering onto a 1.1-M sucrose solution in Buffer 4 (350 μL) and subjecting the mixture to ultracentrifugation at 540,000 × g for 90 min at 4 °C. The POST5 pellet was resuspended and subjected to a second identical ultracentrifugation to remove trace residual eEF2 that could interfere with subsequent assays. The final pellet was dissolved in Buffer 4 and stored in small aliquots at −80 °C for at least 3 mo with no discernible loss of activity. POST5 complexes used in octapeptide formation assays were prepared using [^{3}H]-Gln-tRNA^{Gln}. For fluorescence studies, [^{14}C]-Gln-tRNA^{Gln} was used.

[^{3}H]-Trp-PRE6 and [^{3}H]-Trp-POST6 complexes. The procedure was adapted from Zhang et al. (39). Trp-PRE6 was formed by incubating 100 μL of 0.05 μM Trp-POST5, 0.5 μM [^{3}H]Trp-tRNA^{Trp}, 1 μM eEF1A, and 1 mM GTP for 30 s at 37 °C. Trp-POST6 was formed similarly but with 1 μM eEF2 added. Trp-PRE6 and Trp-POST6 were purified by ultracentrifugation as described for POST5 complexes.

Assays. All assays were performed in Buffer 4 at 37 °C. All concentrations in the legends for Figs. 2 to 5 and *SI Appendix*, Figs. S1 to S3 are final after mixing. In assays involving ribosome pelleting, carrier 70S *E. coli* ribosomes (100 pmol, 3 μL of 33-μM 70S) were added. The resulting mixtures were layered onto a 1.1-M sucrose solution in Buffer 4 (350 μL), and the mixture was subject to ultracentrifugation at 540,000 × g for 70 min at 4 °C.

eRF1/eRF3-dependent pentapeptidyl-tRNA hydrolysis, hexapeptide formation, hexapeptidyl-tRNA dissociation, and octapeptide formation. Each of these assays was performed on a POST5 complex.

eRF1/eRF3-dependent pentapeptidyl-tRNA hydrolysis was determined using two methods to measure the formation of pentapeptide following incubation of Stop-POST5 containing P-site bound FKVR[^{3}H]Q-tRNA^{Gln} with eRF1, eRF3, and GTP. In both methods, eRF1 and eRF3 were first preincubated at 37 °C in Buffer 4 for 30 s. The TRID to be tested, or an equivalent buffer volume, was then added to make up to total volume of 20 μL. A total of 20 μL Stop-POST5 preheated to 37 °C was next added to initiate the reaction. The 40-μL reaction mixture contained, as final concentrations, 0.05 μM Stop-POST5, 0.1 μM eRF1, 0.2 μM eRF3, and 1 mM GTP. At various times, the reaction was quenched with 150 μL of 0.5 M MES buffer (pH 6.0) at 0 °C, ribosomes were pelleted as described above, and the ^{3}H radioactivity of supernatant was determined. In method 2, which gave essentially identical results (*SI Appendix*, Fig. S4 *A* and *B*), the pH 6–quenched reaction mixture was lyophilized, dissolved in water, and analyzed by thin-layer electrophoresis (TLE) as previously described, using pH 2.8 running buffer (1, 39). The identity of FKVR[^{3}H]Q pentapeptide was verified by its comigration with authentic FKVRQ pentapeptide obtained from GenScript (Piscataway, NJ). Method 1 was used for the results reported in Fig. 2*D* and *SI Appendix*, Fig. S1 because it was simpler to perform.

Hexapeptide formation was determined by TLE. POST5 complex (0.02 μM) was mixed with [^{3}H]Trp-tRNA^{Trp} (0.04 to 1.5 μM), eEF1A (0.04 to 1.5 μM), eRF1 (0.020 μM), eRF3 (0.040 μM), and 1 mM GTP for times varying from 0.5 s to 10 min in the absence or presence of TRIDs. Reactions were quenched with excess 0.4 M KOH. For slower reactions ($t_{1/2}$ >30 s), mixing and quenching were carried out manually. For faster reactions ($t_{1/2}$ <30 s), mixing and quenching were carried out using a KinTek Corporation RQF-3 Rapid Quench-Flow Instrument. Base-quenched samples were incubated at 37 °C for 2.5 h to completely release hexapeptide FKVRQ[^{3}H]W from tRNA^{Trp}. The supernatant was analyzed by TLE as described previously (1, 39). The identity of FKVRQ[^{3}H]W hexapeptide was confirmed (*SI Appendix*, Fig. S4*C*) by the comigration of ^{3}H radioactivity with authentic FKVRQW hexapeptide obtained from GenScript (Piscataway, NJ).

Hexapeptidyl-tRNA dissociation was determined by incubating POST5 complex (0.02 μM) with [^{3}H]Trp-tRNA^{Trp} (0.5 μM), eEF1A (1.0 μM), and 1 mM GTP in a 40-μL reaction mixture for various times, quenching the reaction at pH 6 and at 0 °C, and determining the FKVRQ[^{3}H]W-tRNA^{Trp} in the ribosomal pellet following ultracentrifugation.

Octapeptide formation from POST5 complexes was determined as described previously (1).

Puromycin assay. We determined the reactivities toward puromycin (5 μM) of 0.025 μM each of [^{3}H]-Trp-PRE6, [^{3}H]-Trp-POST6, or [^{3}H]-Trp-PRE6 plus an addition of 1 μM eEF2 and GTP (1 mM). Aliquots (40 μL) were quenched at various times with 150 μL 0.5-M MES buffer at pH 6.0 and at 0 °C, and the FKVRQ[^{3}H]W-tRNA^{Trp} remaining in the ribosomal pellet was determined.

Trp-tRNA^{Trp}(prf) binding and PRE6 translocation assays. Prf-labeled Trp-TC, formed by preincubating 0.05 μM Trp-tRNA^{Trp}(prf), 2.0 μM eEF1A, and 1 mM GTP, was rapidly mixed with various concentrations of either Trp-POST5 or Stop-POST5 in the absence of TRID or in the presence of either 10 μM G418 or 500 μM ataluren. The fluorescence change during the reaction was monitored on a Kintek SF-300X stopped-flow spectrofluorometer as described earlier (58, 59). Proflavin in Trp-tRNA^{Trp}(prf) was excited at 462 nm, and the emission was monitored using a 515 ± 15 nm band-pass filter. The translocation assay was performed identically, except that 1 to 3 μM eEF2 was added to the POST5 complex.

Calculations of free variable reactant concentrations. Free concentrations of reactants for results presented in Fig. 3 *C* and *D* were calculated using an iterative procedure, as follows. Free concentrations of POST5, [E], were initially estimated by [E] = $[E]_T$ − $[S]_T$, where $[E]_T$ and $[S]_T$ represent total added POST5 and Trp-TC, respectively. The dependence of the apparent rate constant of tRNA association ($k_{app,1}$) on [E] is given by Eq. **4**:

$$k_{app,1} = k_1[E] + k_{-1}. \quad [4]$$

The dissociation constant $K_D = k_{-1}/k_1$ was determined from plots Eq. **4**. The value of K_D permitted calculation of [ES] (Eq. **5**) and hence of [E], equal to $[E]_T$ − [ES], allowing

$$[ES] = \frac{([E]_T + [S]_T + K_D) - \sqrt{\left([E]_T + ([S]_T + K_D)^2 - 4[E]_T[S]_T\right.}}{2} \quad [5]$$

updated calculations of k_1, k_{-1}, and K_D. This process was repeated until the values of these parameters were unchanged. These values are listed in Table 2.

Calculations of free concentrations in Fig. 4*B* of Trp-TC, [S], were performed similarly using an initial estimate of [S] = $[S]_T$ − $[E]_T$. The apparent rate constants of hexapeptide formation ($k_{app,pep}$) were fitted into the Michaelis–Menten equation (60):

$$k_{app,pep} = \frac{k_{pep}[S]}{K_{m,pep} + [S]}. \quad [6]$$

[ES] was calculated using $K_{m,pep}$ with an equation similar to Eq. **5** but with K_D replaced by $K_{m,pep.}$ The final, stable values of k_{pep} and $K_{m,pep.}$ are listed in Table 2.

Data Availability. All study data are included in the article and *SI Appendix*.

ACKNOWLEDGMENTS. We thank Wesley Friesen (PTC Therapeutics, TRIDs) and Allan Jacobson and Alper Celik (University of Massachusetts Medical School, yeast eRF1 and eRF3 plasmids and purified proteins) for reagents used in these studies. This work was supported by research grants to B.S.C. (PTC Therapeutics; Cystic Fibrosis Foundation-COOPER18G0; and NIH GM127374) and Y.E.G. (NIH GM118139).

1. M. Y. Ng *et al.*, New *in vitro* assay measuring direct interaction of nonsense suppressors with the eukaryotic protein synthesis machinery. *ACS Med. Chem. Lett.* **9**, 1285–1291 (2018).
2. S. Brenner, A. O. W. Stretton, S. Kaplan, Genetic code: The 'nonsense' triplets for chain termination and their suppression. *Nature* **206**, 994–998 (1965).
3. M. Shalev, T. Baasov, When proteins start to make sense: Fine-tuning aminoglycosides for PTC suppression therapy. *MedChemComm* **5**, 1092–1105 (2014).
4. K. M. Keeling, X. Xue, G. Gunn, D. M. Bedwell, Therapeutics based on stop codon readthrough. *Annu. Rev. Genomics Hum. Genet.* **15**, 371–394 (2014).
5. F. Salvatori *et al.*, Production of β-globin and adult hemoglobin following G418 treatment of erythroid precursor cells from homozygous β(0)39 thalassemia patients. *Am. J. Hematol.* **84**, 720–728 (2009).
6. T. Goldmann *et al.*, A comparative evaluation of NB30, NB54 and PTC124 in translational read-through efficacy for treatment of an USH1C nonsense mutation. *EMBO Mol. Med.* **4**, 1186–1199 (2012).
7. P. D. Stenson *et al.*, The human gene mutation database: Towards a comprehensive repository of inherited mutation data for medical research, genetic diagnosis and next-generation sequencing studies. *Hum. Genet.* **136**, 665–677 (2017).
8. M. Mort, D. Ivanov, D. N. Cooper, N. A. Chuzhanova, A meta-analysis of nonsense mutations causing human genetic disease. *Hum. Mutat.* **29**, 1037–1047 (2008).
9. K. Nagel-Wolfrum, F. Möller, I. Penner, T. Baasov, U. Wolfrum, Targeting nonsense mutations in diseases with translational read-through-inducing drugs (TRIDs). *BioDrugs* **30**, 49–74 (2016).
10. A. Leier *et al.*, Mutation-directed therapeutics for neurofibromatosis type I. *Mol. Ther. Nucleic Acids* **20**, 739–753 (2020).
11. N. Oishi *et al.*, XBP1 mitigates aminoglycoside-induced endoplasmic reticulum stress and neuronal cell death. *Cell Death Dis.* **6**, e1763 (2015).
12. N. Siddiqui, N. Sonenberg, Proposing a mechanism of action for ataluren. *Proc. Natl. Acad. Sci. U.S.A.* **113**, 12353–12355 (2016).

13. L. Bidou, O. Bugaud, V. Belakhov, T. Baasov, O. Namy, Characterization of new-generation aminoglycoside promoting premature termination codon readthrough in cancer cells. *RNA Biol.* **14**, 378–388 (2017).
14. M. Jospe-Kaufman, L. Siomin, M. Fridman, The relationship between the structure and toxicity of aminoglycoside antibiotics. *Bioorg. Med. Chem. Lett.* **30**, 127218 (2020).
15. D. K. Crawford, I. Alroy, N. Sharpe, M. M. Goddeeris, G. Williams, ELX-02 generates protein via premature stop codon read-through without inducing native stop codon read-through proteins. *J. Pharmacol. Exp. Ther.* **374**, 264–272 (2020).
16. A. Yonath, Antibiotics targeting ribosomes: Resistance, selectivity, synergism and cellular regulation. *Annu. Rev. Biochem.* **74**, 649–679 (2005).
17. D. N. Wilson, The A-Z of bacterial translation inhibitors. *Crit. Rev. Biochem. Mol. Biol.* **44**, 393–433 (2009).
18. G. M. Blaha, Y. S. Polikanov, T. A. Steitz, Elements of ribosomal drug resistance and specificity. *Curr. Opin. Struct. Biol.* **22**, 750–758 (2012).
19. T. Pape, W. Wintermeyer, M. V. Rodnina, Conformational switch in the decoding region of 16S rRNA during aminoacyl-tRNA selection on the ribosome. *Nat. Struct. Biol.* **7**, 104–107 (2000).
20. K. B. Gromadski, M. V. Rodnina, Streptomycin interferes with conformational coupling between codon recognition and GTPase activation on the ribosome. *Nat. Struct. Mol. Biol.* **11**, 316–322 (2004).
21. A. Tsai *et al*., The impact of aminoglycosides on the dynamics of translation elongation. *Cell Rep.* **3**, 497–508 (2013).
22. J. Zhang, M. Y. Pavlov, M. Ehrenberg, Accuracy of genetic code translation and its orthogonal corruption by aminoglycosides and Mg^{2+} ions. *Nucleic Acids Res.* **46**, 1362–1374 (2018).
23. N. Garreau de Loubresse *et al*., Structural basis for the inhibition of the eukaryotic ribosome. *Nature* **513**, 517–522 (2014).
24. I. Prokhorova *et al*., Aminoglycoside interactions and impacts on the eukaryotic ribosome. *Proc. Natl. Acad. Sci. U.S.A.* **114**, E10899–E10908 (2017).
25. Y. Shimizu, T. Kanamori, T. Ueda, Protein synthesis by pure translation systems. *Methods* **36**, 299–304 (2005).
26. K. Machida *et al*., A translation system reconstituted with human factors proves that processing of encephalomyocarditis virus proteins 2A and 2B occurs in the elongation phase of translation without eukaryotic release factors. *J. Biol. Chem.* **289**, 31960–31971 (2014).
27. E. Jan, T. G. Kinzy, P. Sarnow, Divergent tRNA-like element supports initiation, elongation, and termination of protein biosynthesis. *Proc. Natl. Acad. Sci. U.S.A.* **100**, 15410–15415 (2003).
28. A. M. Lancaster, E. Jan, P. Sarnow, Initiation factor-independent translation mediated by the hepatitis C virus internal ribosome entry site. *RNA* **12**, 894–902 (2006).
29. S. Inge-Vechtomov, G. Zhouravleva, M. Philippe, Eukaryotic release factors (eRFs) history. *Biol. Cell* **95**, 195–209 (2003).
30. D. C. Soares, P. N. Barlow, H. J. Newbery, D. J. Porteous, C. M. Abbott, Structural models of human eEF1A1 and eEF1A2 reveal two distinct surface clusters of sequence variation and potential differences in phosphorylation. *PLoS One* **4**, e6315 (2009).
31. R. Jørgensen, A. R. Merrill, G. R. Andersen, The life and death of translation elongation factor 2. *Biochem. Soc. Trans.* **34**, 1–6 (2006).
32. R. J. Jackson, C. U. T. Hellen, T. V. Pestova, The mechanism of eukaryotic translation initiation and principles of its regulation. *Nat. Rev. Mol. Cell Biol.* **11**, 113–127 (2010).
33. A. Ferguson *et al*., Functional dynamics within the human ribosome regulate the rate of active protein synthesis. *Mol. Cell* **60**, 475–486 (2015).
34. L. Du *et al*., A new series of small molecular weight compounds induce read through of all three types of nonsense mutations in the ATM gene. *Mol. Ther.* **21**, 1653–1660 (2013).
35. T. Pape, W. Wintermeyer, M. V. Rodnina, Complete kinetic mechanism of elongation factor Tu-dependent binding of aminoacyl-tRNA to the A site of the *E. coli* ribosome. *EMBO J.* **17**, 7490–7497 (1998).
36. M. V. Rodnina, A. Savelsbergh, V. I. Katunin, W. Wintermeyer, Hydrolysis of GTP by elongation factor G drives tRNA movement on the ribosome. *Nature* **385**, 37–41 (1997).
37. A. Savelsbergh *et al*., An elongation factor G-induced ribosome rearrangement precedes tRNA-mRNA translocation. *Mol. Cell* **11**, 1517–1523 (2003).
38. D. Pan, S. V. Kirillov, B. S. Cooperman, Kinetically competent intermediates in the translocation step of protein synthesis. *Mol. Cell* **25**, 519–529 (2007).
39. H. Zhang, M. Y. Ng, Y. Chen, B. S. Cooperman, Kinetics of initiating polypeptide elongation in an IRES-dependent system. *eLife* **5**, e13429 (2016).
40. J. L. Alejo, S. C. Blanchard, Miscoding-induced stalling of substrate translocation on the bacterial ribosome. *Proc. Natl. Acad. Sci. U.S.A.* **114**, E8603–E8610 (2017).
41. E. Gutierrez *et al*., eIF5A promotes translation of polyproline motifs. *Mol. Cell* **51**, 35–45 (2013).
42. A. P. Schuller, C. C.-C. Wu, T. E. Dever, A. R. Buskirk, R. Green, eIF5A functions globally in translation elongation and termination. *Mol. Cell* **66**, 194–205.e5 (2017).
43. W. Liu *et al*., EF-tu dynamics during pre-translocation complex formation: EF-Tu·GDP exits the ribosome via two different pathways. *Nucleic Acids Res.* **43**, 9519–9528 (2015).
44. M. Sokabe, C. S. Fraser, Toward a kinetic understanding of eukaryotic translation. *Cold Spring Harb. Perspect. Biol.* **11**, a032706 (2019).
45. O. Bugaud *et al*., Kinetics of CrPV and HCV IRES-mediated eukaryotic translation using single-molecule fluorescence microscopy. *RNA* **23**, 1626–1635 (2017).
46. M. Dabrowski, Z. Bukowy-Bieryllo, E. Zietkiewicz, Advances in therapeutic use of a drug-stimulated translational readthrough of premature termination codons. *Mol. Med.* **24**, 25 (2018).
47. A. Campofelice *et al*., Strategies against nonsense: Oxadiazoles as translational readthrough-inducing drugs (TRIDs). *Int. J. Mol. Sci.* **20**, 3329 (2019).
48. P. Morais, H. Adachi, Y. T. Yu, Suppression of nonsense mutations by new emerging technologies. *Int. J. Mol. Sci.* **21**, 4394 (2020).
49. M. Borgatti, E. Altamura, F. Salvatori, E. D'Aversa, N. Altamura, Screening read-through compounds to suppress nonsense mutations: Possible application to β-Thalassemia. *J. Clin. Med.* **9**, 289 (2020).
50. B. Roy *et al*., Ataluren stimulates ribosomal selection of near-cognate tRNAs to promote nonsense suppression. *Proc. Natl. Acad. Sci. U.S.A.* **113**, 12508–12513 (2016).
51. S. W. Peltz, M. Morsy, E. M. Welch, A. Jacobson, Ataluren as an agent for therapeutic nonsense suppression. *Annu. Rev. Med.* **64**, 407–425 (2013).
52. D. Kessel, A. Morgan, G. M. Garbo, Sites and efficacy of photodamage by tin etiopurpurin in vitro using different delivery systems. *Photochem. Photobiol.* **54**, 193–196 (1991).
53. S. M. Rabea *et al*., 2-Aminothiazole-4-carboxamides enhance readthrough of premature termination codons by aminoglycosides. *ACS Med. Chem. Lett.* **10**, 726–731 (2019).
54. R. Jørgensen, A. Carr-Schmid, P. A. Ortiz, T. G. Kinzy, G. R. Andersen, Purification and crystallization of the yeast elongation factor eEF2. *Acta Crystallogr. D Biol. Crystallogr.* **58**, 712–715 (2002).
55. A. Celik, "mRNA decay pathways use translation fidelity and competing decapping complexes for substrate selection," PhD thesis, Microbiology and Physiological Systems, University of Massachusetts Medical School, Worcester, MA (2017).
56. D. Pan, S. Kirillov, C.-M. Zhang, Y.-M. Hou, B. S. Cooperman, Rapid ribosomal translocation depends on the conserved 18-55 base pair in P-site transfer RNA. *Nat. Struct. Mol. Biol.* **13**, 354–359 (2006).
57. D. Pan, H. Qin, B. S. Cooperman, Synthesis and functional activity of tRNAs labeled with fluorescent hydrazides in the D-loop. *RNA* **15**, 346–354 (2009).
58. W. Liu, D. Shin, Y. Tor, B. S. Cooperman, Monitoring translation with modified mRNAs strategically labeled with isomorphic fluorescent guanosine mimetics. *ACS Chem. Biol.* **8**, 2017–2023 (2013).
59. W. Liu *et al*., Stringent nucleotide recognition by the ribosome at the middle codon position. *Molecules* **22**, 1427 (2017).
60. L. Michaelis, M. Menten, Die kinetik der Invertinwirkung. *Biochem. Z.* **49**, 333–369 (1913).